ISSN 2616-5872 Vol.7, Issue 3: 73-79, DOI: 10.25236/AJEE.2025.070310

# An Improved Parameterization Scheme for All-Sky Broadband Sea Surface Albedo Weighted by Solar Zenith Angle and Atmospheric Transmittance

**Zijian Zhang[1,a], Hanwen Ling[1,b], Zhiyong Jiao[1,c]**

*[1]College of Science, China University of Petroleum (East China), Qingdao, 266580, China*
*[a]zzj18886340556@gmail.com, [b]1094420560@qq.com, [c]jiaozhy@upc.edu.cn*

***Abstract:*** *Ocean surface albedo (OSA) significantly influences air-sea heat exchanges and Earth's radiative balance, but accurately modeling it remains challenging due to high environmental variability. We propose a novel broadband parameterization integrating solar zenith angle and atmospheric transmittance, enabling seamless representation across clear-sky and overcast conditions. Coefficients were derived via nonlinear fitting to comprehensive observational data from the northern South China Sea. The parameterization demonstrates strong performance ($R = 0.892$, $RMSE = 0.0132$) and is independently validated using historical datasets from the North Atlantic and Central Pacific ($R \geq 0.75$, $RMSE \leq 0.061$). Residual analysis highlights secondary influences of wind speed, wave height, and humidity, indicating potential refinements. This physically interpretable and computationally efficient model is particularly suitable for climate simulations, radiative transfer studies, and remote sensing applications.*

***Keywords:*** *Ocean Surface Albedo, Broadband Parameterization, Solar Zenith Angle, Atmospheric Transmittance, Radiative Transfer, Climate Modeling*

## 1. Introduction

Incoming solar radiation at the ocean surface is divided into absorption by the water column and reflection to the atmosphere. The fraction reflected, known as ocean surface albedo, is critical for regulating air–sea heat exchange and Earth's radiative balance. Compared to land or ice surfaces, OSA is relatively low—typically 0.03–0.10 under mid-range conditions—but ranges nearly an order of magnitude, from approximately 0.01 for smooth, sunlit seas to more than 0.45 in whitecap-covered breaking waves[1][2][3]. Capturing this variability is essential for climate simulations, since upper-ocean heating and sea surface temperature are highly sensitive to the balance between absorbed and reflected solar energy [4].

However, field measurement of OSA remains technically challenging. The upwelling shortwave irradiance just above a moving sea surface is weak and prone to contamination [2]. In contrast, downwelling radiation is routinely observed, which necessitates the use of parameterizations to estimate reflected fluxes based on readily available inputs[5][6].Over the past decades, numerous OSA parameterizations have been proposed. Early models assume idealized conditions, treating the ocean as a flat Fresnel reflector under direct-beam incidence. These approaches capture the primary dependence on solar zenith angle, but ignore the effects of wave slope, atmospheric scattering, and sky condition. Later, empirical schemes incorporate observed datasets. Notably, Briegleb et al[7]use ship-based measurements from Payne to derive a clear-sky OSA expression as a function of SZA. While more realistic, this "legacy" formula is limited to direct-beam, cloud-free conditions. Hansen et al[8] introduce a wind-dependent formulation using surface slope statistics from the Cox–Munk distribution[9]. More sophisticated models later include aerosol/cloud effects and water-column properties; for example, Jin et[10] aldevelop a lookup-table scheme based on SZA, transmittance, wind, and ocean chlorophyll.

While complex models can achieve high accuracy, their reliance on rarely available inputs limits practicality, creating a persistent gap between simple, widely applicable schemes and comprehensive, data-intensive ones[11]. Several representative parameterizations illustrate this trade-off. Fresnel's law expresses the angular reflectance of a flat water surface:

$$\alpha = \frac{1}{2}\left[\frac{\sin^2(\eta-\xi)}{\sin^2(\eta+\xi)} + \frac{\tan^2(\eta-\xi)}{\tan^2(\eta+\xi)}\right] \quad (1)$$

ISSN 2616-5872 Vol.7, Issue 3: 73-79, DOI: 10.25236/AJEE.2025.070310

Where $\eta$ is the solar incident angle and $\xi = \arcsin(\sin\eta/1.33)$ is the refracted angle in water. To account for oceanic effects, Briegleb et al. (1986) proposed:

$$\alpha = \frac{0.026}{\mu^{1.7}+0.065} + 0.15(\mu - 0.1)(\mu - 0.5)(\mu - 1) \quad (2)$$

Where $\mu = \cos\theta$. Taylor et al. (1996) offered a simplified fit:

$$\alpha = \frac{0.037}{1.1\mu^{1.4}+0.15} \quad (3)$$

While effective under clear skies, these schemes lack adaptability to cloudy or mixed-sky conditions and omit key atmospheric and oceanic factors.

Recent observational studies reveal how OSA varies under diverse sky and sea states. Under clear skies, OSA rises steeply with increasing SZA, especially at low Sun angles, while in cloudy conditions, it remains nearly constant (approximately 0.02–0.05), as diffuse illumination smooths angular effects. Surface roughness enhances albedo by increasing effective incidence angles, whereas elevated atmospheric humidity reduces it by absorbing near-infrared energy. Experiments confirm that higher wind speeds and wave heights raise albedo, while increased vapor pressure reduces it in a roughly linear fashion [12].

These findings have motivated a new generation of semi-empirical parameterizations. Some recent models distinguish clear versus cloudy regimes using atmospheric transmittance (β) as a blending factor, with optional corrections for wind and humidity. Others predict all-sky OSA as an analytical function of solar angle and surface irradiance, achieving correlations of approximately 0.90 and RMSD of 0.013 when validated against multi-season data[13]. Meanwhile, GCM-compatible schemes have emerged, such as spectral OSA models based on ocean chlorophyll, though at the cost of higher input complexity. These developments underscore the need for an approach that is both physically based and operationally feasible.

In this context, a broadband OSA parameterization is proposed that balances physical rigor with practical simplicity. The scheme relies on two core variables—solar geometry ($\mu = \cos\theta$) and atmospheric transmittance—to represent albedo variability under both clear and cloudy conditions in a unified framework. These inputs can be readily derived from routine measurements, and the formulation remains analytically simple and computationally efficient. All coefficients are empirically fit to observational data and recalibrated in this study to enhance generalizability. The resulting scheme provides accurate, continuous estimates of ocean surface albedo across a wide range of sky conditions and is well suited for applications in climate models and radiative transfer diagnostics.

## 2. Observations and Datasets

The FIO OSA dataset utilized for the development of the parameterization scheme in this study is publicly available on Zenodo (Huang et al., 2023). Observational data were collected at a fixed offshore platform in the northern South China Sea (21.44°N, 111.39°E) (Figure. 1). Detailed descriptions of the instrumentation and data processing procedures are provided in Huang et al. (2023). A Kipp & Zonen CNR4 four-component net radiometer was installed approximately 6 meters above mean sea level to measure broadband downward and upward shortwave irradiances (305–2800 nm). The sea surface albedo (α) for each measurement period was calculated as

$$\alpha = \frac{Q_{up}}{Q_{down}} \quad (4)$$

Where $Q_{up}$ and $Q_{down}$ denote the upward and downward broadband shortwave irradiances, respectively. Additional meteorological parameters, including wind speed and air humidity (from which surface vapor pressure, $e^0$, was derived), were recorded by co-located instruments on the tower. A downward-facing acoustic Doppler current profiler deployed on the sea floor provided significant wave height ($H_s$) as an indicator of sea state. Radiation data were collected as 30-minute averages.Quality-control procedures followed published guidelines. Periods during which the platform infrastructure shadowed the radiometers were excluded. Observations with solar altitude less than 10° (i.e., solar zenith angle $\theta > 80°$) were omitted, as very low Sun angles often yield unstable albedo measurements. Additionally, records with extremely low downwelling irradiance (< 30 W m$^{-2}$) were discarded to avoid large fractional errors when the incident flux approached zero.After filtering, a total of 2,433 half-hour segments remained for analysis, spanning September 2017 to December 2018 and covering multiple seasons and a wide range of sky conditions. The final dataset includes synchronized measurements of

ISSN 2616-5872 Vol.7, Issue 3: 73-79, DOI: 10.25236/AJEE.2025.070310

$Q_{down}$, $Q_{up}$ (Figure. 2), wind speed, wave height, and vapor pressure (Figure. 3), providing an ideal basis for developing and testing the albedo parameterization scheme.

*Figure 1 The sea platform in the northern South China Sea (viewed fromthe northeast). The instrument in the red circle is the CNR4 used in this paper.*

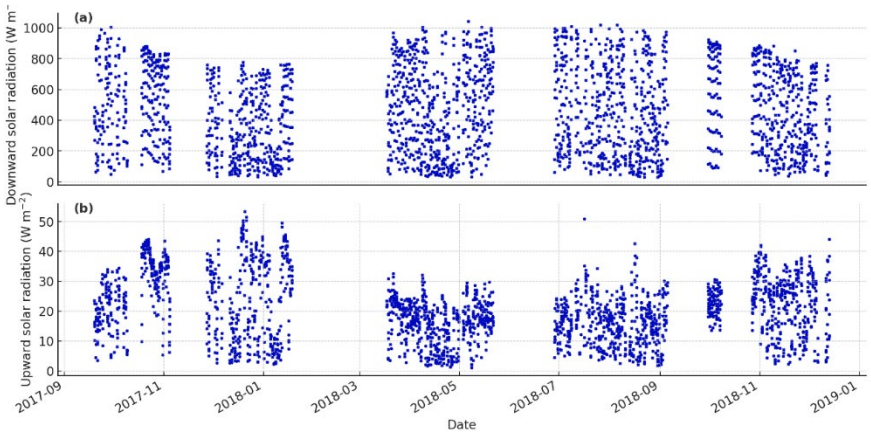


*Figure 2 Time series of (a) downward and (b) upward broadband shortwave radiation measured at the FIO offshore tower in the northern South China Sea from September 2017 to December 2018.*

## 3. Broadband Albedo Parameterization Scheme

### *3.1 Rationale for the Functional Form*

Ocean surface albedo is governed by both solar geometry and atmospheric conditions. While previous studies have shown that clear skies result in a strong dependence on solar zenith angle, whereas overcast skies exhibit little such dependence, the aim here is to formally capture this dual-regime behaviour in a single expression. To this end, two physically interpretable predictors are adopted: the cosine of SZA, $\mu = \cos\theta$, and the atmospheric transmittance, $\beta$, defined as the fraction of top-of-atmosphere irradiance reaching the surface. The parameter $\beta$ serves as a proxy for the relative dominance of direct versus diffuse radiation: high $\beta$ implies clear-sky, beam-dominated conditions, whereas low $\beta$ reflects diffusely-lit, cloud-covered skies. This motivates the formulation of albedo as a $\beta$-weighted blend between a $\mu$-dependent direct-beam term and a constant diffuse baseline.

In this study, the atmospheric transmittance $\beta$ is defined as the ratio of surface downward shortwave radiation, $Q_d$, to the theoretical top-of-atmosphere irradiance, $Q_{\text{top}}$:

$$\beta = \frac{Q_d}{Q_{\text{top}}} \tag{5}$$

The quantity $Q_{\text{top}}$ is computed as the solar irradiance incident at the top of the atmosphere under clear-sky conditions:

$$Q_{\text{top}} = \frac{S_0}{d^2}\cos\theta \tag{6}$$

ISSN 2616-5872 Vol.7, Issue 3: 73-79, DOI: 10.25236/AJEE.2025.070310

Where $S_0 = 1361\ \mathrm{W\,m^{-2}}$ is the solar constant, $\theta$ is the solar zenith angle, and $d$ is the normalized Earth–Sun distance for the given day of year (DOY). The distance factor $d$ is calculated by:

$$d = 1 + 0.0167\sin\left(\frac{2\pi(\mathrm{DOY}-93.5)}{365}\right) \tag{7}$$

This formulation accounts for the annual variation in Earth–Sun distance and solar geometry, ensuring accurate estimation of clear-sky irradiance and thus enabling consistent derivation of $\beta$ throughout the observation period.

The derivation of the parameterisation follows a four-step physical rationale. First, the measured transmittance $\beta$ is used to decompose the total incoming shortwave flux into direct and diffuse components, with respective fractional weights $\beta$ and $1-\beta$. This provides an energy-based weighting structure. Second, the direct-beam albedo is modelled as a function of solar zenith angle via the empirical expression $\alpha_{\mathrm{dir}}(\mu) = A/(\mu^p + B)$, capturing the observed increase in reflectance at low Sun angles. Third, in heavily overcast conditions where diffuse radiation dominates, the albedo is observed to approach a nearly constant value, typically around $C \approx 0.05$, which is adopted as the diffuse baseline. These three components are then combined into a single expression through linear superposition. The total albedo is expressed as a weighted sum of direct and diffuse components, with weights proportional to their energy fractions. This formulation is justified by radiative flux conservation: since albedo is defined as the ratio of reflected to total incident flux, and the direct and diffuse streams are assumed to interact independently with the ocean surface, the total albedo becomes:

$$\alpha = \frac{Q_{\mathrm{dir}}\alpha_{\mathrm{dir}} + Q_{\mathrm{dif}}\alpha_{\mathrm{dif}}}{Q_{\mathrm{dir}} + Q_{\mathrm{dif}}} = \beta\alpha_{\mathrm{dir}} + (1-\beta)C \tag{8}$$

Where $\beta = Q_{\mathrm{dir}}/Q_{\mathrm{tot}}$ and $\alpha_{\mathrm{dif}} = C$. Thus, the energy-partitioning $\{\beta, 1-\beta\}$ provides a natural set of linear weights that retain both physical fidelity and mathematical simplicity.

Substituting the angular expression for $\alpha_{\mathrm{dir}}$ and the constant $C$ yields the final broadband albedo parameterization:

$$\alpha(\mu, \beta) = \beta\frac{A}{\mu^p + B} + (1-\beta)C \tag{9}$$

Where $A$, $B$, $C$, and $p$ are empirical coefficients, estimated via nonlinear regression in Section 3.2. In the limit $\beta \to 1$, corresponding to clear-sky conditions, the expression reduces to the direct-beam term,capturing the strong angular dependence. In the limit $\beta \to 0$, the expression reduces to the constant baseline, consistent with a nearly angle-independent albedo under diffuse lighting. The use of a rational function for the direct component allows flexible tuning of angular response, while the constant $C$ supplies a physically reasonable lower bound under uniformly cloudy skies.

In summary, Equation (9) embodies a physically interpretable and energy-conserving blend of angular reflectance and diffuse background, yielding a compact, continuous approximation that encompasses both clear and overcast regimes within a single parameterisation scheme.

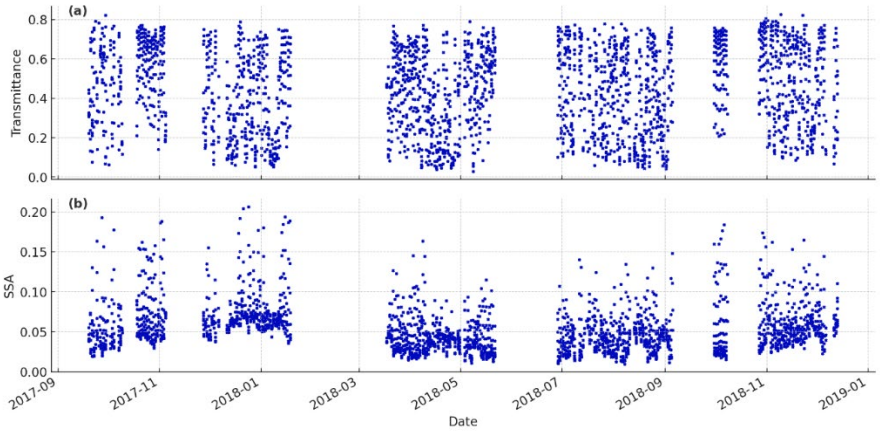


*Figure 3 Time series of (a) atmospheric transmittance $\beta$ and (b) broadband ocean surface albedo derived from FIO tower observations from September 2017 to December 2018.*

ISSN 2616-5872 Vol.7, Issue 3: 73-79, DOI: 10.25236/AJEE.2025.070310

### *3.2 Parameter Estimation Procedure*

The coefficients A,B,C, and p in Equation (9) were obtained by nonlinear least-squares fitting to observed albedo data from the South China Sea offshore platform. Each half-hourly data point provided measured albedo, along with corresponding μ and β. Before fitting, the data underwent quality control to exclude periods of sensor malfunction or shading.Parameter fitting used the Levenberg–Marquardt algorithm, initialized with physically reasonable values based on previous studies ,C near 0.05, p ≈ 1.5, A ≈ 0.03–0.04, B ≈ 0.1. The algorithm iteratively adjusted the parameters to minimize the sum of squared errors, with convergence typically reached in under 100 iterations.To estimate parameter uncertainties, block-bootstrap resampling was performed by resampling daily data segments 1,000 times. Fitting was repeated for each bootstrap sample, and 95% confidence intervals were derived from the resulting parameter distributions, accounting for time correlations within the data.

### *3.3 Optimized Parameter Values and Physical Interpretation*

The optimisation yielded a well-constrained set of coefficients for Equation (9). Table.1 summarises the final values of $A$, $B$, $C$, and $p$ along with their 95 % confidence intervals from the bootstrap analysis. All parameters are significant and physically plausible. The fitted model achieved an excellent match to the observations across all sky conditions (overall correlation $R = 0.892$ and root-mean-square error RMSE = 0.0132, comparable to measurement uncertainty), and does not exhibit systematic bias in any particular regime. Figure 4 shows the overall performance of the fitted scheme. Panel (a) shows a scatterplot of modelled versus observed albedo values, with the 1:1 line for reference. Panel (b) presents the empirical cumulative distribution function (CDF) of the prediction error $(\alpha_{\mathrm{obs}} - \alpha_{\mathrm{mod}})$, indicating that approximately 88 % of the errors fall within ±0.02. Together, these diagnostics confirm that the parameterisation reproduces the observed variability with high accuracy and minimal bias.

*Table 1 Optimized coefficients for the broadband-albedo scheme (Equation 9) with 95 % confidence intervals.*

| Parameter | Optimized Value | 95 % Confidence Interval |
|---|---|---|
| A | 0.0170 | 0.0158 – 0.0182 |
| B | 0.0407 | 0.0379 – 0.0436 |
| C | 0.0476 | 0.0463 – 0.0490 |
| P | 2.98 | 2.84 – 3.11 |

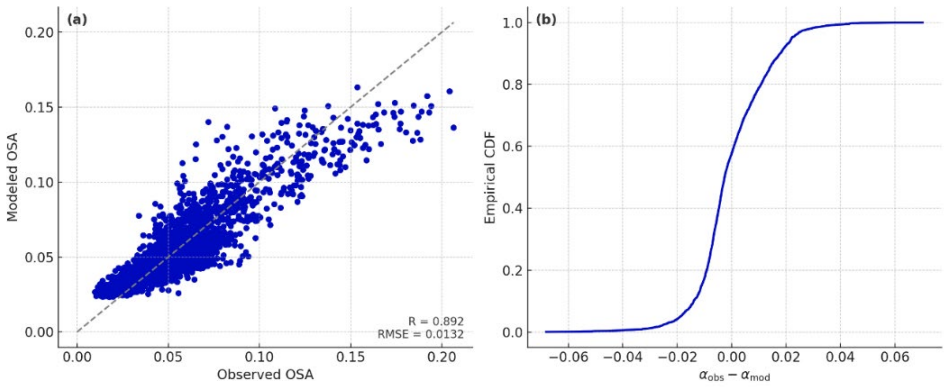


*Figure 4 (a) Scatter-plot comparison of observed ocean surface albedo (OSA) and OSA modeled using Eq. (10) under all-sky conditions. The grey line denotes the 1:1 reference line. (b) Empirical cumulative distribution function (ECDF) of the deviation ε between observed and modeled OSA.*

### *3.4 Optimized Parameter Values and Physical Interpretation*

Figure 5 summarizes the relationships between the residuals ( $\varepsilon = \alpha_{\mathrm{obs}} - \alpha_{\mathrm{sim}}$ ) and three environmental variables: (a) wind speed at 10 m height ($U_{10}$), (b) significant wave height ($H_s$), and (c) near-surface vapor pressure ($e_0$). As shown in Figure 5a–b, higher wind speeds and increased wave heights tend to result in larger residuals, likely because enhanced whitecap formation and foam locally increase reflectance; however, these two factors together account for less than 12% of the previously unexplained variance. In contrast, Figure 5c reveals a slight negative relationship, indicating that higher humidity modestly reduces the residuals, explaining less than 4% of the variance. The temporal evolution

ISSN 2616-5872 Vol.7, Issue 3: 73-79, DOI: 10.25236/AJEE.2025.070310

and overall range of these three factors during the 16-month observation period are illustrated in Figure 6a–c, highlighting intermittent occurrences of elevated $U_{10}$ and $H_s$ and clear seasonal variations in $e_0$. Although incorporating linear correction terms based on $U_{10}$, $H_s$, and $e_0$ could further reduce the residual scatter, such additional complexity is deferred to future refinements of the parameterization scheme.

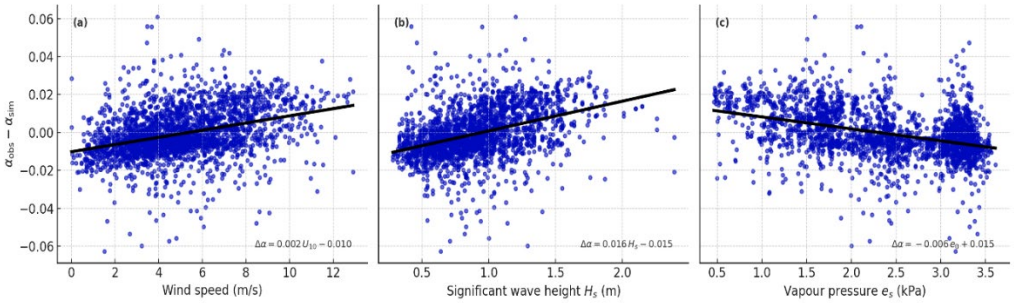


*Figure 5 Residuals $(\alpha_{obs} - \alpha_{sim})$ as a function of (a) wind speed, (b) wave height, and (c) vapor pressure, with black linear fits and regression equations.*

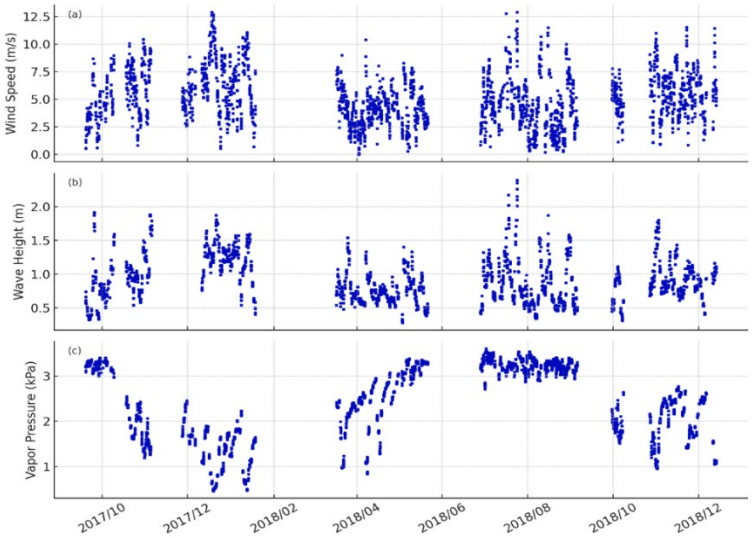


*Figure 6 Time series of three environmental parameters measured at the FIO offshore platform from September 2017 to December 2018: (a) 10 m wind speed, (b) significant wave height, and (c) near-surface vapor pressure.*

## 4. Conclusions

This study introduces a novel four-parameter broadband ocean surface albedo parameterisation, specifically designed for oceanographic and climate modelling applications. The formulation blends a physically motivated angular-reflectance term dependent on solar zenith angle with a diffuse baseline, weighted by atmospheric transmittance, enabling seamless transitions between clear-sky and overcast conditions. Calibration using comprehensive South China Sea observational data confirmed the scheme's statistical robustness and physical interpretability. Residual analyses highlighted subtle yet systematic effects from secondary environmental factors, including wind speed, wave height, and humidity, suggesting opportunities for further refinement. Overall, the developed parameterisation offers a simple, physically grounded, and accurate approach suitable for satellite remote sensing, radiative transfer analyses, and coupled climate simulations.

## References

*[1] Payne R E. Albedo of the sea surface[J]. Journal of Atmospheric Sciences, 1972, 29(5): 959–970.*
*[2] Katsaros K B, McMurdie L A, Lind R J, et al. Albedo of a water surface: spectral variation, effects of atmospheric transmittance, sun angle and wind speed[J]. Journal of Geophysical Research: Oceans,*

ISSN 2616-5872 Vol.7, Issue 3: 73-79, DOI: 10.25236/AJEE.2025.070310

*1985, 90(C4): 7313–7321.*
*[3] Koepke P. Effective reflectance of oceanic whitecaps[J]. Applied Optics, 1984, 23(11): 1816–1824.*
*[4] Cess R D, Goldenberg S L. The effect of ocean diurnal variations on climate sensitivity[J]. Journal of Geophysical Research: Oceans, 1981, 86(C11): 10919–10922.*
*[5] Hogikyan A, Cronin M F, Zhang D, et al. Uncertainty in net surface heat flux due to differences in commonly used albedo products[J]. Journal of Climate, 2020, 33(1): 303–315.*
*[6] Chen H, Jiang B, Li R, et al. Evaluation of the J-OFURO3 sea surface net radiation and inconsistency correction[J]. Remote Sensing, 2021, 13(20): 4170.*
*[7] Briegleb B P, Minnis P, Ramanathan V, et al. Comparison of regional clear-sky albedos inferred from satellite observations and model computations[J]. Journal of Climate and Applied Meteorology, 1986, 25(2): 214–226.*
*[8] Hansen J, Russell G, Rind D, et al. Efficient three-dimensional global models for climate studies: Models I and II[J]. Monthly Weather Review, 1983, 111(4): 609–662.*
*[9] Cox C, Munk W. Measurement of the roughness of the sea surface from photographs of the Sun's glitter[J]. Journal of the Optical Society of America, 1954, 44(11): 838–850.*
*[10] Jin Z, Charlock T P, Smith W L Jr, et al. A parameterization of ocean surface albedo[J]. Geophysical Research Letters, 2004, 31(22): L22301.*
*[11] Dickinson R E. Land surface processes and climate—surface albedos and energy balance[J]. Advances in Geophysics, 1983, 25: 305–353.*
*[12] Preisendorfer R W, Mobley C D. Albedos and glitter patterns of a wind-roughened sea surface[J]. Journal of Physical Oceanography, 1986, 16(7): 1293–1316.*
*[13] Wei J, Ren T, Yang P, et al. An improved ocean surface albedo computational scheme: structure and performance[J]. Journal of Geophysical Research: Oceans, 2021, 126(7): e2020JC016958.*